Influence of doping on the spin dynamics and magnetoelectric effect in hexagonal $Y_{0.7}Lu_{0.3}MnO_3$

W. Tian,[1,*] Guotai Tan,[2,3,†] Liu Liu,[2] Jinxing Zhang,[2] Barry Winn,[1] Tao Hong,[1] J. A. Fernandez-Baca,[1,3] Chenglin Zhang,[3,4] and Pengcheng Dai[3,4]

[1]*Quantum Condensed Matter Division, Oak Ridge National Laboratory, Oak Ridge, Tennessee 37831, USA*

[2]*Department of Physics, Beijing Normal University, Beijing 100875, China*

[3]*Department of Physics and Astronomy, The University of Tennessee, Knoxville, Tennessee 37996, USA*

[4]*Department of Physics and Astronomy, Rice University, Houston, Texas 77005, USA*

(Received 9 August 2013; revised manuscript received 3 April 2014; published 18 April 2014)

We use inelastic neutron scattering and dielectric constant measurements to study the doping influence on the spin dynamics and magnetoelectric (ME) effect in hexagonal $Y_{0.7}Lu_{0.3}MnO_3$. In undoped $YMnO_3$ and $LuMnO_3$, the Mn trimerization distortion has been suggested to play a key role in determining the magnetic structure and the magnetoelectric effect. In $Y_{0.7}Lu_{0.3}MnO_3$, at the antiferromagnetic zone center, we observed a much smaller $\Delta_{12} \approx 0.52$ meV gap (which is ~2.5 meV for both $YMnO_3$ and $LuMnO_3$) that coincides with a weaker in-plane dielectric anomaly at T_N; both can be attributed to a weaker Mn trimerization distortion in $Y_{0.7}Lu_{0.3}MnO_3$ compared to $YMnO_3$ and $LuMnO_3$. The results provide strong evidence that the magnitude of ME coupling is linked to the strength of the trimerization distortion, suggesting the Mn trimerization is responsible for the ME effect in $Y_{1-y}Lu_yMnO_3$.

DOI: 10.1103/PhysRevB.89.144417 PACS number(s): 75.85.+t, 75.30.Ds, 75.40.Gb, 75.50.Ee

Driven by modern technology trends towards device miniaturization, there is considerable interest in multiferroic materials, which exhibit both magnetic order and electrical polarization [1–7]. The hexagonal manganite $RMnO_3$ [8,9] (where R is a rare-earth element with relatively small ionic radius) is a prototypical example of the so-called type-I multiferroics [10] with ferroelectric order at $T_c \sim 900$ K [11] and an antiferromagnetic (AFM) order at much lower temperature, $T_N \sim 100$ K [12]. A large dielectric anomaly occurs at T_N [13–15] indicating strong magnetoelectric (ME) coupling in these materials. There has been a large amount of experimental work in recent years, with the aim to understand the microscopic mechanism for the coupling between magnetic and electric degrees of freedom in these materials. Although it is generally believed that the spin-lattice coupling plays an important role in determining the complex properties in $RMnO_3$, much is unclear concerning the factors that influence the magnitude of the ME coupling [16,17]. In the present paper, we use inelastic neutron scattering (INS) and dielectric constant measurements to show that the magnitude of the ME coupling is directly coupled to the strength of the Mn trimerization distortion in $Y_{0.7}Lu_{0.3}MnO_3$ in the AFM phase. Our results thus provide strong evidence that the Mn trimerization is responsible for the ME effect and multiferroic phenomenon in $Y_{1-y}Lu_yMnO_3$.

Undoped $YMnO_3$ and $LuMnO_3$ are characteristic hexagonal manganites with the Mn^{3+} ions at the $x \sim 1/3$ position forming a nearly ideal triangular lattice in the ab plane above T_N. $YMnO_3$ and $LuMnO_3$ undergo AFM transitions (to two different magnetic structures) at $T_N \sim 75$ K and $T_N \sim 88$ K respectively, accompanied by an isostructural transition with large atomic displacement for all atoms in the unit cell. In particular, a distinct change of the Mn atomic position, namely the Mn trimerization distortion, occurs in the basal plane at T_N [17]. As illustrated in Fig. 1, the Mn trimers distort in opposite directions in $YMnO_3$ and $LuMnO_3$, expanding for $YMnO_3$ and contracting for $LuMnO_3$. A recent theoretical study finds that the different magnetic structures of $YMnO_3$ and $LuMnO_3$ are determined by the different trimerization directions in these compounds [18]. Moreover, the dielectric anomaly at T_N is observed only in ε_{ab} but not in ε_c for both $YMnO_3$ and $LuMnO_3$ [15]. Although these studies suggest that the Mn trimerization may play a key role in determining the magnetic structure and the ME effects in $Y_{1-y}Lu_yMnO_3$, there are no experimental studies to determine the connection between the Mn trimerization and ME coupling. $Y_{1-y}Lu_yMnO_3$ is an ideal system for such a study due to the following reasons: (1) since both Y and Lu are nonmagnetic, $Y_{1-y}Lu_yMnO_3$ is a clean system to study the magnetism of the Mn triangular lattice and its correlation with the ME effects; (2) the strength of the Mn trimerization distortion can be tuned in $Y_{1-y}Lu_yMnO_3$. At 10 K, with increasing Lu concentration y, the Mn atomic position x changes from 0.340 for $YMnO_3$, larger than $x_c = 1/3$ for an ideal triangular lattice, to 0.331 for $LuMnO_3$, smaller than 1/3. At $y \sim 0.3$, the Mn atomic position x is very close to the critical value $x_c = 1/3$; we thus expect a much weaker trimerization distortion in $Y_{0.7}Lu_{0.3}MnO_3$ [19].

All measurements reported here were performed on single-crystal samples. Large $Y_{1-y}Lu_yMnO_3$ single crystals with nominal value of $y = 0.3$ were grown by the floating zone method under 4 atmospheres of oxygen flow. The crystals cut from the long rods were then annealed at 1350 °C for 24 hours in a flowing argon atmosphere. For the magnetic susceptibility and dielectric constant measurements, the single crystal was cut into thin plates with ab axes lying in the plane and the c axis pointing out of the plane. The magnetic susceptibility was measured using a Quantum Design magnetic properties measurement system with magnetic field applied along the c axis. The dielectric constant was measured using an inductance-capacitance-resistance (LCR) meter with electric field applied perpendicular and parallel to the c axis, and data were taken at 3.5 V ac driving voltage and 100 kHz frequency.

*wt6@ornl.gov

†tanbj2008@gmail.com

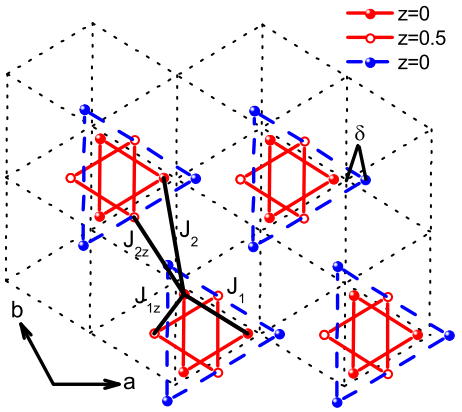

FIG. 1. (Color online) Schematic drawing of the Mn trimerization distortion below T_N. The dotted line depicts the ideal triangular lattice in the hexagonal ab plane with Mn ions at the $x_c = 1/3$ position. The solid blue and red circles represent Mn ions in the $z = 0$ plane, illustrating the opposite distortion directions of the Mn trimers: expansion in $YMnO_3$ (blue) and contraction in $LuMnO_3$ (red). For $LuMnO_3$, the Mn ions in the $z = 0.5$ plane are shown as red open circles, and the in-plane (J_1,J_2) and interplane (J_{1z},J_{2z}) magnetic exchange interactions are shown by solid lines. $\delta = |x\text{-}x_c|$ is the trimerization distortion parameter as described in the text.

A single crystal with a mass of ∼4 grams was used for the neutron scattering experiments. The crystal was mounted on a aluminum plate and oriented in the (H 0 L) scattering plane. The sample was then sealed in aluminum sample can under helium atmosphere and cooled using a closed-cycle He refrigerator. The neutron experiments were carried out using the HB-1A and CTAX triple-axis spectrometers (TAS) located at the High Flux Isotope Reactor (HFIR), and the Hybrid Spectrometer (HYSPEC) located at the Spallation Neutron Source (SNS) at Oak Ridge National Laboratory. HB-1A is a fixed incident energy TAS ($E_i = 14.64$ meV), and CTAX is a cold neutron TAS. Collimations of 48′-48′-sample-40′-80′ downstream from the reactor to the detector was used for the HB-1A experiment with two pyrolitic graphite (PG) filters placed before the sample to eliminate higher-order contaminations in the beam. The CTAX experiment was performed with a fixed final energy of $E_f = 3$ meV (energy resolution is ∼0.1 meV FWHM at elastic condition) and collimations of guide-open-sample-80′-open. Higher-order contaminations were removed by a cooled Be filter placed between the sample and the analyzer. The HYSPEC experiment was carried out using an incident energy of $E_i = 25$ meV with a Fermi chopper spinning at 420 Hz.

The $Y_{0.7}Lu_{0.3}MnO_3$ crystal was characterized by the magnetic susceptibility and neutron scattering magnetic order parameter measurements. Figure 2(a) shows the magnetic susceptibility measured with $H \parallel c$ exhibiting a kink at ∼78 K indicating the AFM transition. The order parameter plotted in Fig. 2(b) was measured by monitoring the strong magnetic Bragg peak (1 0 1) as a function of temperature. The integrated intensity was obtained by fitting the (1 0 1) rocking curve measured at each temperature to a Gaussian function with a constant background. As illustrated by the dashed green line, the AFM transition at $T_N \sim 78$ K was observed in

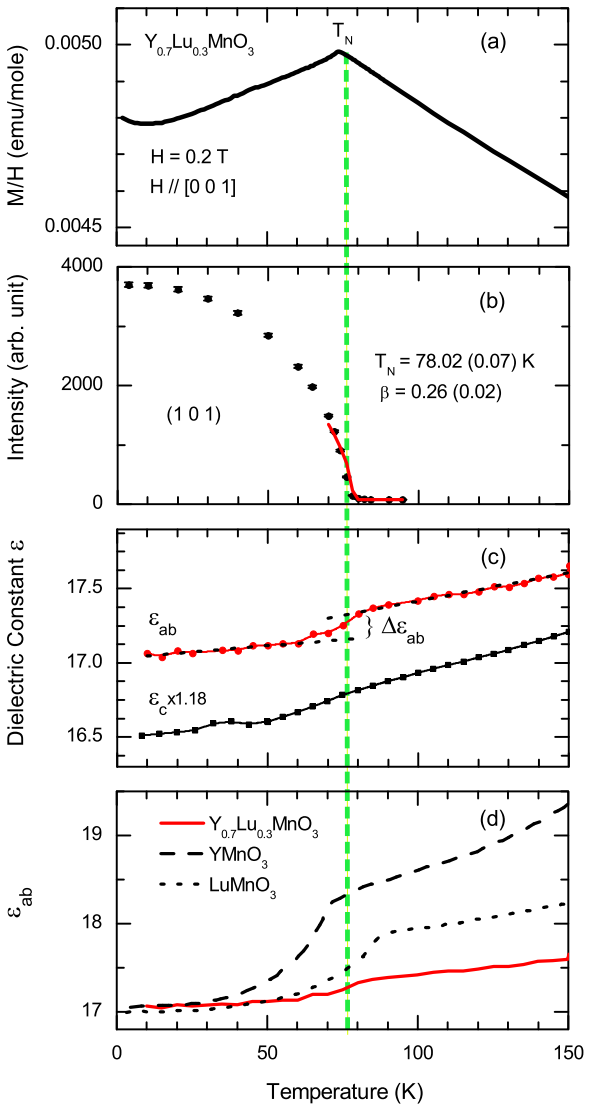

FIG. 2. (Color online) Magnetic susceptibility, magnetic order parameter, and dielectric constant measurements of $Y_{0.7}Lu_{0.3}MnO_3$. The dashed green line depicts the Neel temperature T_N. (a) Magnetic susceptibility versus temperature measured with applied magnetic field parallel to the c axis. (b) Integrated intensity of the (1 0 1) magnetic Bragg reflection as a function of temperature. The solid red line is a fit of the data to the power law as described in the text. (c) In-plane and out-of-plane dielectric constant measured with the electric field applied perpendicular and parallel to the c axis. $\Delta\varepsilon_{ab}$ defines the critical in-plane dielectric constant change at T_N. (d) Comparison of the in-plane dielectric constant ε_{ab} between $YMnO_3$, $LuMnO_3$, and $Y_{0.7}Lu_{0.3}MnO_3$. The data for $YMnO_3$ ($\varepsilon_{ab} - 2.1$) and $LuMnO_3$ ($\varepsilon_{ab} + 0.3$) are from Ref. [15] and are plotted with offsets of −2.1 and 0.3 for $YMnO_3$ and $LuMnO_3$, respectively.

both measurements, consistent with previous reports [19]. The solid red line in Fig. 2 (b) is a fit to a power-law $I(T) = I_0[(T_N - T)/T_N)]^{2\beta}$ that yields $T_N \approx 78.02 \pm 0.07$ K and $\beta \approx 0.26 \pm 0.02$, where β is the critical exponent. The yielded $\beta \sim 0.26$ value is between the theoretical values of a two-dimensional ($\beta = 0.125$) and a three-dimensional ($\beta = 0.326$) Ising systems, in good agreement with a prior study [20].

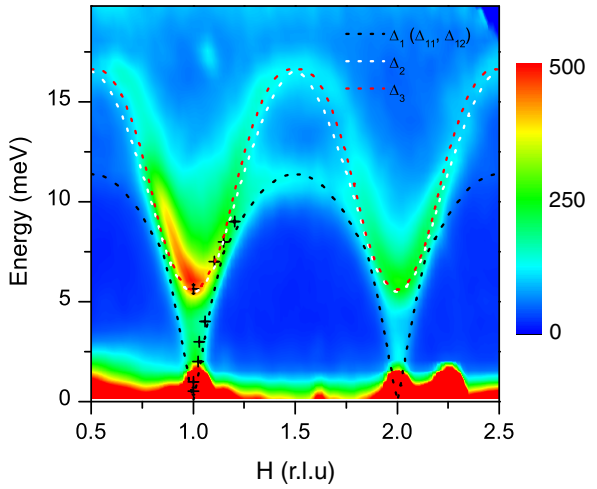

FIG. 3. (Color online) INS spectra of $Y_{0.7}Lu_{0.3}MnO_3$ along (H 0 0) from the HYSPEC measurements at 4 K. The crossed symbols are data points obtained from TAS measurements. The dotted lines are the calculated dispersion (six branches appear as three doubly degenerate branches) from the spin-wave model as described in the text.

The spin dynamics of Mn^{3+} ions has been investigated in detail in $YMnO_3$, $LuMnO_3$, and $HoMnO_3$ [20–24]. There are six Mn^{3+} ions in the magnetic unit cell that lead to six magnon branches in these materials. However, due to the fact that the interplane magnetic coupling is much weaker compared to the in-plane magnetic exchange interaction, the spin-wave dispersion in the hexagonal ab plane appears as three branches (Δ_1, Δ_2, and Δ_3 as depicted in Fig. 3), each containing two nearly doubly degenerate modes [23,24]. Only the degeneracy of the Δ_1 low energy branch can be lifted at the zone center [becoming Δ_{11} and Δ_{12} as shown in Figs. 4(a) and 4(b)] and along L due to interlayer coupling. Figure 3 shows the INS spectra of $Y_{0.7}Lu_{0.3}MnO_3$ projected along the (H 0 0) direction, where the crossed symbols are data points from TAS measurements, in good agreement with the HYSPEC data. Figure 4 summarizes the TAS data measured along L. As shown in Figs. 4(a)–4(c), at the magnetic zone center, two modes were observed in $Y_{0.7}Lu_{0.3}MnO_3$, $\Delta_{12} \approx 0.52$ meV [Fig. 4(b)] and $\Delta_3 (\approx \Delta_2) \approx 5.56$ meV [Fig. 4 (c)], whereas the lowest energy mode $\Delta_{11} \approx 0$ meV [Fig. 4 (a)] is gapless within instrumental resolution (~0.1 meV FWHM at elastic condition). In comparison, previous study has shown that $\Delta_{11} \approx 0.22$ meV, $\Delta_{12} \approx 2.4$ meV, and $\Delta_3 \approx 5.4$ meV in $YMnO_3$ [20,23]; and $\Delta_{11} \approx 0$ meV, $\Delta_{12} \approx 2.5$ meV, and $\Delta_3 \approx 6.5$ meV in $LuMnO_3$ [24]. Figure 4(d) plots the derived dispersion curves along L by fitting the energy scans at constant wave vector, assuming Gaussian peak shape. Similar to that reported for $YMnO_3$ and $LuMnO_3$, strong dispersions were observed along H (Fig. 3) with an overall bandwidth of ~17 meV (which is ~16 and 21 meV for $YMnO_3$ and $LuMnO_3$), and weak dispersions were observed along L [Fig. 4 (d)] consistent with the layered magnetic structure of $Y_{1-y}Lu_yMnO_3$. The ~5.5 meV mode (containing four degenerate modes from upper Δ_2 and Δ_3 branches) is dispersionless along L within the instrumental resolution. Overall, the q dependence of the magnetic spectra of $Y_{0.7}Lu_{0.3}MnO_3$ shows very similar behavior compared to $YMnO_3$ and $LuMnO_3$, except that unlike $YMnO_3$ and $LuMnO_3$ which have almost the same value of $\Delta_{12} \approx 2.5$ meV regardless of the opposite trimerization distortion direction in these materials, a much smaller $\Delta_{12} \approx 0.52$ meV was observed in $Y_{0.7}Lu_{0.3}MnO_3$.

In order to make a quantitative comparison between $YMnO_3$, $Y_{0.7}Lu_{0.3}MnO_3$, and $LuMnO_3$, we analyze the observed $Y_{0.7}Lu_{0.3}MnO_3$ spin-wave dispersion using the same model that has been applied to $YMnO_3$ in Ref. [23] and $LuMnO_3$ in Ref. [24]. The spin Hamiltonian can be described by the following equation:

$$\mathcal{H} = -\sum_{\langle ij \rangle} J_{ij}\vec{S}_i \cdot \vec{S}_j - D_1 \sum_i \left(S_i^z\right)^2 - D_2 \sum_i (\vec{S}_i \cdot \vec{n}_i)^2, \quad (1)$$

which takes into account two in-plane (J_1,J_2) and two interplane (J_{1z},J_{2z}) exchange interactions as depicted in Fig. 1, and D_1 and D_2 represent the out-of-plane and in-plane anisotropies. The direction of the in-plane anisotropy D_2 is parallel to the spin directions, $\vec{n}_i = \langle \vec{S}_i \rangle / |\langle \vec{S}_i \rangle|$. Using the program implemented in the MCPHASE software package [25], a fit to the $Y_{0.7}Lu_{0.3}MnO_3$ data yields $J_1 = -2.65(5)$ meV, $J_2 = -2.32(5)$ meV, $J_{2z} = 0.0012(4)$ meV, and $D_1 = -0.44(1)$ meV under the following constraints: (1) Our neutron diffraction measurements show that $Y_{0.7}Lu_{0.3}MnO_3$ adopted the same magnetic structure as $LuMnO_3$, thus the same spin-wave model used for $LuMnO_3$ [24] in the MCPHASE package can be applied to analyze the $Y_{0.7}Lu_{0.3}MnO_3$ data. (2) The in-plane anisotropy D_2 term is needed in $YMnO_3$ because of the $\Delta_{11} \approx 0.22$ meV gap, but it can be set to $D_2 = 0$ in $Y_{0.7}Lu_{0.3}MnO_3$ and $LuMnO_3$ because the Δ_{11} gap is too small to be detected. (3) As shown in Figs. 3 and 4(d), the degeneracy of the Δ_1 mode is lifted and becomes Δ_{11} and Δ_{12} at the zone center and along L due to the interplane coupling [23,24], whereas the upper $\Delta_2 \approx \Delta_3$ mode remains degenerate, which precludes J_{1z} and J_{2z} being determined independently [23,24]; therefore $J_{1z} = 0$ is fixed and we obtain the difference of $|J_{1z} - J_{2z}|$ from the fitting. As illustrated in Fig. 3 comparing the calculated results to the measured magnetic spectra, our INS data can be well described by this model.

In Table I we list the fitted parameters for $Y_{0.7}Lu_{0.3}MnO_3$ in comparison with those for $YMnO_3$ and $LuMnO_3$. It shows that the lattice constants, T_N, and D_1 values of $Y_{0.7}Lu_{0.3}MnO_3$ fall in between the values of $YMnO_3$ and $LuMnO_3$, consistent with the fact that both the lattice parameters and the unit cell volume are contracted from $YMnO_3$ to $LuMnO_3$. On the other hand, $J_1 \approx J_2$ is obtained, and in particular a significantly smaller $|J_{1z} - J_{2z}| \approx 0.0012$ (meV), at least 10 times smaller compared to $YMnO_3$ and $LuMnO_3$, is obtained in $Y_{0.7}Lu_{0.3}MnO_3$. We will discuss below that the smaller $\Delta_{12} \approx 0.52$ meV gap observed in $Y_{0.7}Lu_{0.3}MnO_3$ is associated with the weaker Mn trimerization distortion in this material.

The analytic expressions of the energy gaps at the magnetic zone center have been given in a previous study [23] for the spin Hamiltonian [Eq. (1)] assuming very weak interplane

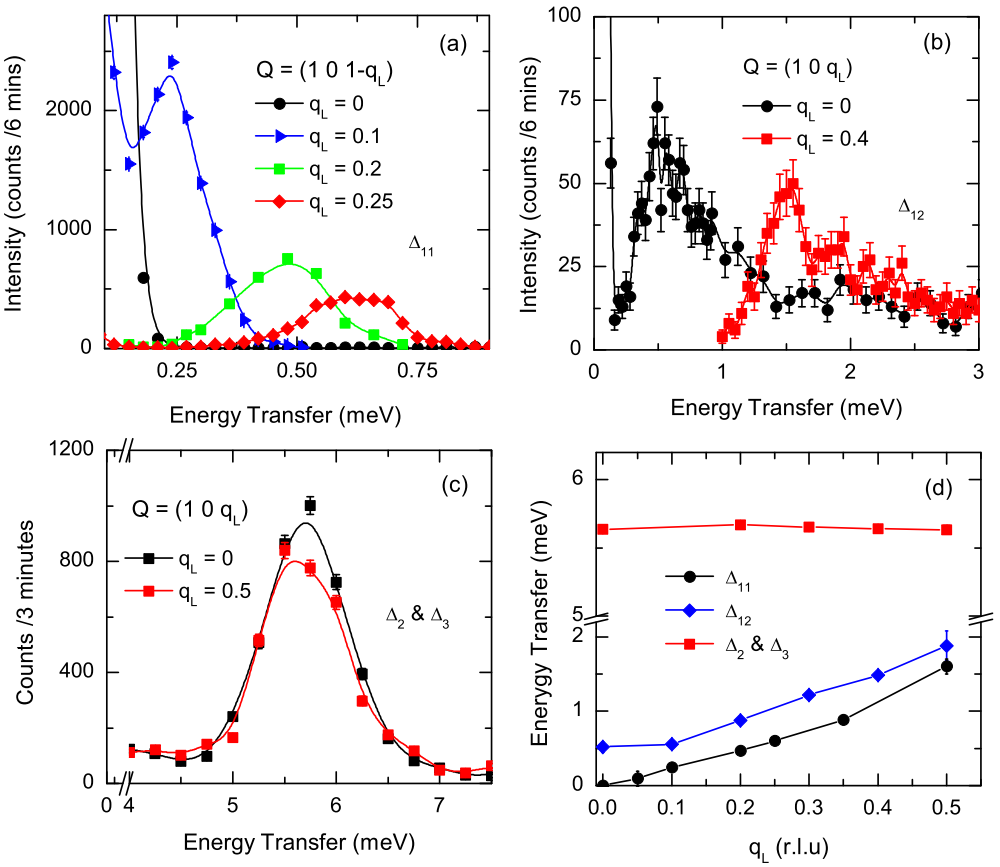

FIG. 4. (Color online) TAS data measured at 4 K illustrates the q dependence of the magnetic excitations along L in $Y_{0.7}Lu_{0.3}MnO_3$. (a) The Δ_{11} gapless mode measured at selected (1 0 1 − q_L) and (b) the $\Delta_{12} \approx 0.52$ meV mode measured at selected (1 0 q_L) using the CG-4C cold neutron TAS. (c) The $\Delta_2 \approx \Delta_3 \approx 5.56$ meV mode measured at selected (1 0 q_L) using the HB-1A thermal neutron TAS. (d) Spin-wave dispersion along the L direction constructed from a series of energy scans at constant wave vector.

couplings J_{1z} and J_{2z}, and in-plane anisotropy D_2:

$$\Delta_{11} \simeq 2S\sqrt{-D_2\lambda_1},$$

$$\Delta_{12} \simeq 2S\sqrt{-D_2\lambda_1 - 2(J_{1z} - J_{2z})\lambda_1},$$

$$\Delta_2 \simeq S\sqrt{2(D_1\lambda_2 - D_2\lambda_3 - 2D_1J_{1z})},$$

$$\Delta_3 \simeq S\sqrt{2[D_1\lambda_2 - D_2\lambda_3 - D_1(J_{1z} - 4J_{2z}) - 2(J_{1z} - J_{2z})\lambda_2]},$$

where λ_1, λ_2 and λ_3 are defined as $\lambda_1 = D_1 + (3/2)J_1 + 3J_2$, $\lambda_2 = (3/2)J_1 + 3J_2$, and $\lambda_3 = 2D_1 + (3/2)J_1 + 3J_2$, respectively. As indicated in the above equation, the Δ_{12} gap is determined by λ_1, D_2, and $J_{1z} - J_{2z}$. Based on the obtained fitting parameters listed in Table I, λ_1 is almost the same between the three compounds: $\lambda_1 = -11.44$, -11.375, and -11.235 meV for $YMnO_3$, $Y_{0.7}Lu_{0.3}MnO_3$, and $LuMnO_3$, respectively. Due to $D_2 \approx 0.0007$ meV being very small for $YMnO_3$, and $D_2 = 0$ being fixed for $Y_{0.7}Lu_{0.3}MnO_3$ and $LuMnO_3$, the $D_2\lambda_1$ term in the Δ_{12} equation can be neglected ($D_2\lambda_1 = 0$ for $Y_{0.7}Lu_{0.3}MnO_3$ and $LuMnO_3$, and $D_2\lambda_1 = 0.008$ for $YMnO_3$). Therefore the $\Delta_{12} \approx 0.52$ meV

TABLE I. Comparison of the lattice constants (space group $P6_3cm$), T_N, in-plane exchange constants J_1 and J_2, difference between interplane exchange couplings $|J_{1z}$-$J_{2z}|$, out-of-plane and in-plane anisotropy parameters D_1 and D_2, trimerization distortion parameter δ, and the critical dielectric constant change parameter $\Delta\varepsilon_{ab}$ between $YMnO_3$, $LuMnO_3$, and $Y_{0.7}Lu_{0.3}MnO_3$.

	$YMnO_3$ (Ref. [23])	$Y_{0.7}Lu_{0.3}MnO_3$ (this work)	$LuMnO_3$ (Ref. [24])
Lattice (Å)	$a = 6.132$, $c = 11.452$	$a = 6.103(2)$, $c = 11.403(1)$	$a = 6.05$, $c = 11.4$
T_N (K)	75	78	88
J_1 (meV)	−3.4 (2)	−2.65 (5)	−4.09 (2)
J_2 (meV)	−2.02 (7)	−2.32 (5)	−1.54 (5)
$\lvert J_{1z} - J_{2z}\rvert$ (meV)	0.014 (2)	0.0012 (4)	0.019(2)
D_1 (meV)	−0.28 (1)	−0.44 (1)	−0.48 (1)
D_2 (meV)	0.0007 (6)	0	0
δ	0.007	0.001	0.003
$\Delta\varepsilon_{ab}$	1.02	0.17	0.77

gap observed in $Y_{0.7}Lu_{0.3}MnO_3$ is due to a much smaller $|J_{1z} - J_{2z}|$. The differences between both in-plane and interplane exchange constants $J_1 - J_2$ and $J_{1z} - J_{2z}$ can serve as good parameters that are very sensitive to the strength of the trimerization distortion, regardless of the small differences in lattice parameters. Smaller $J_1 - J_2$ and $J_{1z} - J_{2z}$ values correspond to weaker trimerization distortion, with the extreme case of $J_1 - J_2 = 0$ and $J_{1z} - J_{2z} = 0$ for an ideal triangular lattice. The obtained $J_1 - J_2 \approx 0.33$ meV and $J_{1z} - J_{2z} \approx 0.0012$ meV both indicate a much weaker Mn trimerization distortion in $Y_{0.7}Lu_{0.3}MnO_3$, consistent with a previous systematic study showing that the Mn atomic position in $Y_{0.7}Lu_{0.3}MnO_3$ is very close to the critical value $x \sim 1/3$ [19].

Our spin-wave study indicates that the smaller Δ_{12} gap observed in $Y_{0.7}Lu_{0.3}MnO_3$ is associated with the weaker Mn trimerization distortion in this material. A dielectric anomaly was observed in both $YMnO_3$ and $LuMnO_3$; it is thus of great interest to see how the weaker Mn trimerization distortion affects the magnitude of the ME coupling. If the ME effect is directly coupled to the Mn trimerization distortion, we would expect a much weaker in-plane dielectric anomaly in $Y_{0.7}Lu_{0.3}MnO_3$, which is indeed what we observed in the dielectric constant measurements. As illustrated in Fig. 2(c), at T_N no anomaly was observed in ε_c, consistent with previous reports, whereas a weaker dielectric anomaly was observed in ε_{ab}. Figure 2(d) compares the in-plane dielectric constant ε_{ab} between $YMnO_3$, $LuMnO_3$, and $Y_{0.7}Lu_{0.3}MnO_3$ (ε_{ab} values for $YMnO_3$ and $LuMnO_3$ are taken from Ref. [15] and plotted in Fig. 2(d) with -2.1 and 0.3 offsets, respectively) and it clearly shows that the dielectric anomaly in $Y_{0.7}Lu_{0.3}MnO_3$ is much weaker compared to $YMnO_3$ and $LuMnO_3$.

To illustrate how the strength of the trimerization distortion affects spin dynamics (Δ_{12} gap) and the in-plane dielectric anomaly, we define a trimerization distortion parameter $\delta = |x - x_c|$ as depicted in Fig. 1 to reflect the strength of the trimerization distortion. We also define a critical dielectric constant change parameter $\Delta\varepsilon_{ab}$ to represent the magnitude of the ME coupling at T_N. As shown in Fig. 2(c), the $T < T_N$ and $T > T_N$ ε_{ab} data are fit to linear functions, and $\Delta\varepsilon_{ab}$ is determined to be the difference between these two fittings at T_N. The $\Delta\varepsilon_{ab}$ and δ (based on the data reported in Ref. [19]) values are listed in Table I. In Fig. 5, we plot $|J_{1z} - J_{2z}|$ vs δ and $\Delta\varepsilon_{ab}$ vs δ for $YMnO_3$, $Y_{0.7}Lu_{0.3}MnO_3$, and $LuMnO_3$. It shows that both $|J_{1z} - J_{2z}|$ and $\Delta\varepsilon_{ab}$ decrease with decreasing δ, indicating strong correlations between the strength of trimerization distortion and the magnitude of ME coupling.

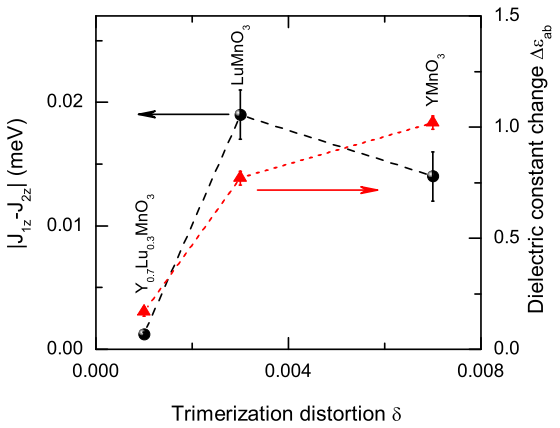

FIG. 5. (Color online) $|J_{1z} - J_{2z}|$ versus trimerization distortion δ (circle, left axis), and critical dielectric constant change $\Delta\varepsilon_{ab}$ versus δ (triangle, right axis) for $Y_{0.7}Lu_{0.3}MnO_3$, $YMnO_3$, and $LuMnO_3$.

In summary, our INS study reveals a smaller Δ_{12} gap that coincides with a weaker ε_{ab} dielectric anomaly in $Y_{0.7}Lu_{0.3}MnO_3$. This is attributed to a much weaker Mn trimerization distortion due to the doping influence: the Mn atomic position x in $Y_{0.7}Lu_{0.7}MnO_3$ is very close to $x_c = 1/3$. These results provide strong evidence that the magnitude of ME coupling is linked to the strength of the trimerization distortion, suggesting the Mn trimerization is responsible for the ME effect in $Y_{1-y}Lu_yMnO_3$. Since a high-resolution neutron diffraction study has shown that the Mn trimerization is a systematic feature in $RMnO_3$ [26], our finding may shed light on a deeper understanding of the multiferroic phenomenon in this series of materials, inviting further theoretical investigations.

We acknowledge valuable discussions with Randy Fishman. Work at the High Flux Isotope Reactor and Spallation Neutron Source, Oak Ridge National Laboratory, was sponsored by the Scientific User Facilities Division, Office of Basic Energy Sciences, U.S. Department of Energy. The single crystal growth and neutron scattering work at UTK/Rice is supported by the US NSF Grants No. DMR-1308603 and No. OISE-0968226. The work at Beijing Normal University was supported by Beijing Natural Science Foundation under Contract No. 2132023; J.Z. also acknowledges the Fundamental Research Funds for the Central Universities (2012LYB07).

[1] M. Fiebig, J. Phys. D: Appl. Phys. **38**, R123 (2005).
[2] N. A. Spaldin and M. Fiebig, Science **309**, 391 (2005).
[3] Y. Tokura, Science **312**, 1481 (2006).
[4] W. Eerenstein, N. D. Mathur, and J. F. Scott, Nature (London) **442**, 759 (2006).
[5] T. Kimura, T. Goto, H. Shintani, K. Ishizaka, T. Arima, and Y. Tokura, Nature (London) **426**, 55 (2003).
[6] N. Hur, S. Park, P. A. Sharma, J. S. Ahn, S. Guha, and S. W. Cheong, Nature (London) **429**, 392 (2004).
[7] S.-W. Cheong and M. Mostovoy, Nat. Mater. **6**, 13 (2007).
[8] M. Fiebig, Th. Lottermoser, D. Fröhlich, A. V. Goltsev, and R. V. Pisarev, Nature (London) **419**, 818 (2002).
[9] T. Lottermoser, T. Lonkai, U. Amann, D. Hohlwein, J. Ihringer, and M. Fiebig, Nature (London) **430**, 541 (2004).
[10] A. B. Harris and G. Lawes, in *The Handbook of Magnetism and Advanced Magnetic Materials* (Wiley, London, 2006).
[11] T. Choi, Y. Horibe, H. T. Yi, Y. J. Choi, W. Wu, and S.-W. Cheong, Nat. Mater. **9**, 253 (2010).

[12] D. G. Tomuta, S. Ramakrishnan, G. J. Nieuwenhuys, and J. A. Mydosh, J. Phys.: Condens. Matter **13**, 4543 (2001).
[13] N. Iwata and K. Kohn, J. Phys. Soc. Jpn. **67**, 3318 (1998).
[14] Z. J. Huang, Y. Cao, Y. Y. Sun, Y. Y. Xue, and C. W. Chu, Phys. Rev. B **56**, 2623 (1997).
[15] T. Katsufuji, S. Mori, M. Masaki, Y. Moritomo, N. Yamamoto, and H. Takagi, Phys. Rev. B **64**, 104419 (2001).
[16] Bas B. Van Aken and Thomas T. M. Palstra, Phys. Rev. B **69**, 134113 (2004).
[17] S. Lee, A. Pirogov, M. Kang, K.-H. Jang, M. Yonemura, T. Kamiyama, S.-W. Cheong, F. Gozzo, N. Shin, H. Kimura, Y. Noda, and J.-G. Park, Nature (London) **451**, 805 (2008).
[18] I. V. Solovyev, M. V. Valentyuk, and V. V. Mazurenko, Phys. Rev. B **86**, 054407 (2012).
[19] J. Park, S. Lee, M. Kang, K.-H. Jang, C. Lee, S. V. Streltsov, V. V. Mazurenko, M. V. Valentyuk, J. E. Medvedeva, T. Kamiyama, and J.-G. Park, Phys. Rev. B **82**, 054428 (2010).
[20] T. Chatterji, S. Ghosh, A. Singh, L. P. Regnault, and M. Rheinstädter, Phys. Rev. B **76**, 144406 (2007).
[21] O. P. Vajk, M. Kenzelmann, J. W. Lynn, S. B. Kim, and S.-W. Cheong, Phys. Rev. Lett. **94**, 087601 (2005).
[22] J. Park, J.-G. Park, G. S. Jeon, H.-Y. Choi, C. Lee, W. Jo, R. Bewley, K. A. McEwen, and T. G. Perring, Phys. Rev. B **68**, 104426 (2003).
[23] T. J. Sato, S.-H. Lee, T. Katsufuji, M. Masaki, S. Park, J. R. D. Copley, and H. Takagi, Phys. Rev. B **68**, 014432 (2003).
[24] H. J. Lewtas, A. T. Boothroyd, M. Rotter, D. Prabhakaran, H. Müller, M. D. Le, B. Roessli, J. Gavilano, and P. Bourges, Phys. Rev. B **82**, 184420 (2010).
[25] M. Rotter *et al.*, MCPHASE, a software package that can calculate the phase diagram and magnetic properties of magnetic materials, 2002–2010, available at http://www.mcphase.de.
[26] X. Fabrèges, S. Petit, I. Mirebeau, S. Pailhès, L. Pinsard, A. Forget, M. T. Fernandez-Diaz, and F. Porcher, Phys. Rev. Lett. **103**, 067204 (2009).